Journal of Aerosol Science 65 (2013) 26–41

Contents lists available at SciVerse ScienceDirect

Journal of Aerosol Science

journal homepage: www.elsevier.com/locate/jaerosci

Particle flow behavior of distribution and deposition throughout 90° bends: Analysis of influencing factors

Ke Sun, Lin Lu*

Department of Building Services Engineering, The Hong Kong Polytechnic University, Hung Hom, Kowloon, Hong Kong SAR 999077, China

ARTICLE INFO

Article history:
Received 22 December 2012
Received in revised form
4 June 2013
Accepted 4 July 2013
Available online 16 July 2013

Keywords:
Particle penetration
Deposition velocity
Concentration distribution
Inlet mass concentration
Reynolds number
Surface material

ABSTRACT

This paper experimentally investigates the particle concentration distribution and deposition in three-dimensional 90° bends considering three potential influencing factors: inlet mass concentration C_m, Reynolds number *Re* and wall material. Particle penetrations were found to decrease moderately within 11% with the increase of C_m under current conditions, but deposition velocity would increase by 1.29–2.87 times. The inlet particle concentration will not affect the outlet concentration distribution and particle penetration for the particles of $St = 5.15 \times 10^{-4}$. For larger particles, however, higher C_m, *St* and *Re* cause higher concentration near the outer wall of bend outlet, lower concentration near the inner wall and even 'particle free zone'. For the outlet concentration distribution, apexes and concave points are observed, which may be formed by the rebounding particles. Furthermore, concentration polarization factor is introduced to analyze the outlet nonuniformity. Accordingly, *Re* is found to be a higher weighting factor compared with C_m. Compared to penetration, deposition velocity is more sensitive to wall materials, for example, with an increase factor up to 1.45. Furthermore, a rough estimation method and an empirical model are suggested to establish the correlation among dimensionless outlet concentration, *St* and 'particle free zone'.

1. Introduction

Particle deposition and distribution in bends is particularly significant for many engineering and environmental applications, including pneumatic conveying (Song et al., 1996; Yang & Kuan, 2006), collecting pollutant samples (Pui et al., 1987), particle treatment in industrial exhaust ducts (Peters & Leith, 2004), solving indoor air quality (IAQ) problems (Chao & Tung, 2001; Li et al., 2007) and controlling particle contaminants for occupants (Jin et al., 2007), especially epidemic ones (Yang et al., 2009). Although particle deposition in ventilation duct has been proved to contribute crucially to filter the contaminants, the deposition and distribution in bend are far from fully understanding.

Particle deposition is influenced by a large amount of factors and changes in a range of one to two orders of magnitudes (Yu et al., 2008; Zhang & Chen, 2009). Disturbed particle flow in bends becomes more complicated for various turbulent flow conditions and particle-wall impactions (Sippola, 2002; Zhang et al., 2010). Raised important factors include particle bulk concentration and its distribution (Zhao & Chen, 2006), Dean number (Lin et al., 2009) and wall materials (Tian et al., 2008; Zhang & Ahmadi, 2000). However, the influences of these factors onto particle distribution and deposition have not been fully studied in bend flows.

* Corresponding author. Tel.: +852 3400 3596; fax: +852 2765 7198.
E-mail addresses: Randal.Soon@gmail.com (K. Sun), vivien.lu@polyu.edu.hk (L. Lu).

0021-8502/$ - see front matter © 2013 Elsevier Ltd. All rights reserved.
http://dx.doi.org/10.1016/j.jaerosci.2013.07.002

Previous studies of particle deposition in ventilation bends focus mainly on averaged penetration and deposition velocity, by both experimental methods (Lai, 2002; McFarland et al., 1997; Peters & Leith, 2004; Pui et al., 1987; Sippola & Nazaroff, 2005; Wilson et al., 2011) and numerical modeling (Berrouk & Laurence, 2008; Breuer et al., 2006; Zaichik et al., 2010). Recent experimental investigations show that depositions are obviously changed by different particle concentration distributions (Lin et al., 2004; Zhao & Wu, 2007, 2009). This is because the concentration distribution alters the particle flux onto a surface. However, the investigations were primarily conducted in chambers and rooms, and the concentration distribution of duct bend should attract more attention. Concentration distribution can also provide the deposition distribution location which the mean deposition values do not reveal.

In practical ventilation environment, the inlet bulk particle concentration varies from time to time under different influencing factors (Zhao & Wu, 2007, 2009). As a result, particle deposition will change with these factors, like inlet concentration. On the other hand, the deposited particles and rebounding particles could influence the concentration distribution at the bend outlet when the inlet concentration varies. The disturbed particle flow in bends will be non-uniform, and thus enhance the deposition on the downstream surfaces of straight ducts (Sippola, 2002; Sippola & Nazaroff, 2005). However, reviewing the literature shows that the interaction between concentration distribution and particle deposition in bends is undiscovered.

Dean number (*De*), as an integration of two dimensionless parameters, e.g. Reynolds number (*Re*) and bend curvature ratio, would be a potential factor to affect particle concentration distribution and deposition. Lin et al. (2009) studied the nanoparticle deposition numerically in curved pipes. The particle deposition over the entire edge of the bent pipe is found to become uniformly-distributed as the *De* increases. Wilson et al. (2011) investigated the effect of high Reynolds number of $Re=10{,}250–30{,}750$ on aerosol deposition, and their results showed that a distinct enhancement in deposition efficiency is detected for $0.1<St<0.4$ when *Re* increases. These recent literature reveal that, however, the Dean number or Reynolds number effect on concentration distribution and concentration-deposition interaction is rare.

To construct the ventilation ducts, series of wall materials can be used according to ASHRAE handbooks (ASHRAE, 2009). Wall material contains significant information of wall characteristics including surface roughness (Tian et al., 2008; Zhang & Ahmadi, 2000) and property of particle-wall collision (Tu et al., 2004). Nevertheless, experimental studies of the wall materials in bend particle flow are seldom found. As a whole, different wall materials are valuable to be investigated.

To further discuss bend particle flow, based on our previous study (Sun et al., 2013), this article aims to: (1) experimentally study the particle concentration spatial distribution in three-dimensional 90° bends; (2) investigate the interaction among particle concentration distribution, penetration and deposition velocity; and (3) analyze potential influencing factors including inlet mass concentration, Reynolds number and wall material.

2. Experimental method

2.1. Definitions

The aerosol deposition efficiency, η, can be defined as

$$\eta=(1-P)100\%=\frac{C_i-C_o}{C_i} \tag{1}$$

where P is aerosol penetration, C_o and C_i are average aerosol number concentration at the bend outlet and inlet respectively. These average concentrations are calculated over all the sampling time period, sampling positions and repeated experiments at each section in this work. Measured penetration through bends are illustrated against particle bend Stokes numbers, *St*, expressed as

$$St=\frac{\tau_p U_{ave}}{(D_h/2)} \tag{2}$$

where U_{ave} is the average air velocity, τ_p is the particle relaxation time, and D_h is the hydraulic diameter of the duct.

The particle deposition velocity expresses the rate of the deposition process, given as

$$V_d=\frac{J_0}{C_{ave}} \tag{3}$$

where J_0 is the deposition flux onto a surface per unit square meter per unit time and C_{ave} stands for the average particle number concentration.

The Reynolds number (*Re*) in the ducts is calculated as

$$Re=\frac{\rho_a U_{ave} D_h}{\mu} \tag{4}$$

where ρ_a is air density and μ is air dynamic viscosity. Based on the Reynolds number, bend Dean number is determined as

$$De=\frac{Re}{\sqrt{R_o}} \tag{5}$$

where R_o is the bend curvature ratio expressed as $(r_1+r_2)/D$. The symbols r_1 and r_2 are interior and outer radii of bend wall, respectively.

2.2. Experimental measurements

Figure 1 demonstrates the measurement setup. The measured bends were of square cross sections with side length $D=10$ cm and of curvature ratio $R_o=3.4$. The duct air velocity upstream was measured at a location of nine duct width ahead of the entrance of the bend by an anemometer (TSI Inc., Model 8386A). The air temperature is 16–20 °C and the density is approximately 1.2 kg/m^3. An aerosol generator (PALAS GmbH, RBG 1000) introduced realistic polydisperse particles (PTI, ISO 12103-1 A2) of 0.7 μm to 100 μm in size far upstream of the test bend. The density of the particle is 2650 kg/m^3. The chemical components of particle are mainly SiO_2 and Al_2O_3. Particle concentrations were sampled at nine uniformly points of the plane of the bend outlet and the inlet to determine the concentrations at these places by an Airborne Particle Counter (Particle Measuring Systems Inc., LASAIR II 310A). Similar procedures were employed in previous studies by other researchers (McFarland et al., 1997; Peters & Leith, 2004). The Airborne Particle Counter (APC) measured six nominal diameters (i.e. 0.3, 0.5, 1, 5, 10, and 25 μm) of particle channels. For each measurement, three groups of repeated data were tested to guarantee the experiment reproducibility. Detail of the experimental approach can be found in the previous research (Sun et al., 2013).

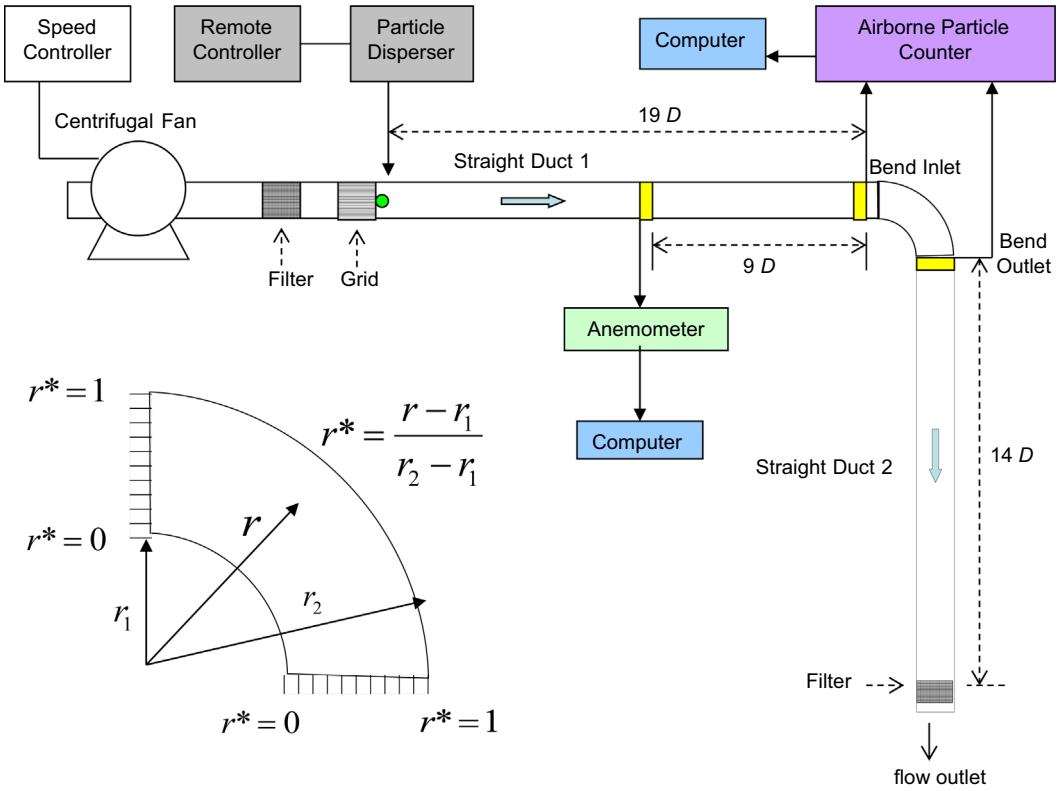

Fig. 1. Schematic diagram of the experimental apparatus (not to scale).

Table 1
Five studied experimental conditions.

Test case no.	Dean number (*De*)	Initial mass concentration (mg/m^3)	Bend wall material
1	9700	11.3	Acrylic glass
2	9700	25.1	Acrylic glass
3	9700	34.5	Acrylic glass
4	19,300	11.3	Acrylic glass
5	9700	34.5	Galvanized steel

Five experimental cases were designed as listed in Table 1 to investigate different condition changes. Reynolds numbers (Re) of 17900 and 35,600 were achieved in the 10 cm square section duct at average velocities of 2.58 m/s and 5.14 m/s, respectively. Correspondingly, Dean numbers (De) were 9700 and 19,300, which is significant parameter for bend flow. Cases 1–3 were designed to compare the influence of inlet mass concentration. Cases 1 and 4 were conducted to study the Reynolds number effect on aerosol particle deposition and distribution. The material difference was investigated under lower Dean number by comparing cases 3 and 5. In addition, all experiments were conducted in horizontal placed bends.

2.3. Data analysis of particle deposition and distribution

The dimensionless particle deposition velocity V_d^+ is presented versus dimensionless relaxation time τ_p^+, computed in the following form:

$$V_d^+ = \frac{V_d}{u_w} = \frac{N_d/A/t_b}{u_w N_0/V} \tag{6}$$

$$\tau_p^+ = \frac{\tau_p}{\tau_e} = \frac{C_c \rho_p d_{pn}^2 u_w^2}{18\,\mu\nu} \tag{7}$$

where V_d is particle deposition velocity; t_b is the maximum flying time scale estimated as $\pi(R_b + D_h/2)/2/U_{ave}$ for each particle through/in the bend; N_0 and N_d mean the numbers respectively of the particles at the bend entrance and those deposited on bend surfaces; A stands for the deposition area and V the bend volume; u_w is the friction velocity of background airflow; τ_p is particle relaxation time; τ_e is the eddy lifetime estimated as ν/u_w^2; ν means air kinematic viscosity; C_c is Cunningham slip correction factor (Sun et al., 2011); ρ_p is particle density; and d_{pn} is measured nominal particle diameter. Similar control volume method has been adopted and tested in the Direction Numerical Simulation (Zhang & Ahmadi, 2000).

Particle concentration distribution, or spatial distribution, for a specific size is normalized by the average concentration $C_{o,St}$ of this size at the symmetric centerline of the bend outlet and inlet, respectively. The dimensionless average concentration $\overline{C}_{r^*}$ at a measurement point of dimensionless wall distance r^* is given as follows

$$C_{o,St} = \frac{1}{m} \sum_{r^* = \frac{1}{m+1}}^{\frac{m}{m+1}} C_{r^*} \tag{8}$$

$$\overline{C}_{r^*} = \frac{C_{r^*}}{C_{o,St}} \tag{9}$$

where C_{r^*} is the average particle concentration over the sampling period and three repeated experiments at a specific dimensionless wall distance r^* and m is the measurement point number, which is nine in this work. For any wall distance as shown in Fig. 1, the r^* is defined as the following expression

$$r^* = \frac{r - r_1}{r_2 - r_1} \tag{10}$$

where the symbol r is the wall distance, and r_1 and r_2 stand for interior and outer radii of bend wall, respectively. The measured nine points locate uniformly at $r^* = 0.1$–0.9 as expressed in Eq. (8). The dimensionless uniform concentration distribution $\overline{C}_u$ for each measurement location is 1.00. Correspondingly, the average deviation is the average value of the absolute deviations of dimensionless concentrations minus $\overline{C}_u$ over the nine locations.

In order to explain the relationship between deposition and concentration distribution, infinitesimal deposition quantity rate dJ of particles at a position are defined based on the control volume concept near the infinitesimal wall surface area dA as deducted in straight duct numerical analysis by Zhao and Chen (2006) and in ventilation room study by Zhao and Wu (2009), which is given as

$$dJ = V_{d,dA} C_{dA} dA \tag{11}$$

$$J = \int_A dJ = \int_A V_{d,dA} C_{dA} dA \tag{12}$$

where $V_{d,dA}$ and C_{dA} are respectively the particle deposition velocity and measured concentration at the adjacent airflow of infinitesimal wall area dA, and J is particle deposition quantity rate. Based on these equations, the average deposition velocity throughout the bends can be determined in Eq. (3). For current horizontally positioned bends of rectangular cross section, the integral Eq. (12) can be divided to

$$J = \int_{Ai} dJ + \int_{Ao} dJ + \int_{Af} dJ + \int_{Ac} dJ = \int_{Ai} V_{d,dAi} C_{dAi} dAi + \int_{Ao} V_{d,dAo} C_{dAo} dAo + \int_{Af} V_{d,dAf} C_{dAf} dAf + \int_{Ac} V_{d,dAc} C_{dAc} dAc \tag{13}$$

where the symbols Ai, Ao, Af and Ac are the deposition area of the inner wall, the outer wall, the floor and the ceiling, respectively; Correspondingly, $V_{d,dAi}$, $V_{d,dAo}$, $V_{d,dAf}$ and $V_{d,dAc}$ are the deposition velocities, and C_{dAi}, C_{dAo}, C_{dAf} and C_{dAc} are the concentration distribution adjacent to the infinitesimal surface. Similarly, other bends with different positioning and cross

section can be deducted based on the above way. In this paper, Eqs. (11)–(13) are adopted to analyze and discuss the correlation between concentration distributions at bend outlet and depositions in bends, especially on inner and outer walls.

3. Results and discussion

3.1. Influence of particle inlet mass concentration on deposition

Different inlet mass concentrations can stand for different particle concentrations of the bend inlet main flow which may affect the deposition near surface boundary layer. Particle concentration at the injection is adjusted accurately by the particle generator to meet the required inlet mass concentration. To find the changing relationship between the inlet concentration and deposition, three mass concentrations (C_m=11.3, 25.1 and 34.5 mg/m^3) were chosen. Accordingly, concentrations throughout the bends were monitored. The measurement was conducted in a 90° bend of clear acrylic glass under Dean number De=9700. The deposition data under C_m=11.3 mg/m^3 in Sun et al. (2013) were adopted here for comparison and analysis. The previous work mainly evaluated the deposition experiment setup and protocol, studied the deposition phenomena and mechanism, and compared literature data and models. Different from our previous study, this subsection focuses on the influence of inlet mass concentration variation onto deposition change.

Figure 2 shows the averaged penetrations against Stokes number under three inlet mass concentrations (C_m=11.3, 25.1 and 34.5 mg/m^3). Considering that concentrations at different locations of a plane perpendicular to the mainstream would be different, particle average penetration was obtained from Eq. (1) and experimental protocol as detailed in Sun et al. (2013) where concentrations were statistically sampled and averaged at bend inlet and outlet plane. Based on the above treatment methods, these averaged concentrations were assumed to be the concentrations at bend inlet and outlet (McFarland et al., 1997; Peters and Leith, 2004). As shown in the figure, measurement standard deviation ranges from 0.2% to 2.6%, which indicate good precisions. The deposition results present that all penetrations decreased with the increase of Stokes number. Small particles with Stokes number $St \leq 5.15 \times 10^{-4}$ had almost fully penetrations through the bend. Particle penetrations reduced moderately within 11% with the increase of inlet mass concentration. The particles with mass concentration C_m=34.5 mg/m^3 had the most and the fastest deposition for different size particles in the bend. For different Stokes numbers, the increasing deposition degrees were different with the increment in initial particle concentration. Deposited particles with Stokes number $St = 1.14 \times 10^{-2}$ increased fast from C_m=11.3 to 25.1 mg/m^3, but the increases for other large particles were relatively smaller. All large particles with Stokes number $St = 1.14 \times 10^{-2}$–0.278 had fast increases of depositions from C_m=25.1 to 34.5 mg/m^3.

Table 2 illustrates the comparison of average dimensionless particle deposition velocity V_d^+ in 90° bends under De=9700 turbulent flow with different inlet mass concentrations. The dimensionless deposition velocity ranged from 0.0905 to 0.567 for dimensionless relaxation time from τ_p^+=0.337 to 8.22 as shown in the table. For C_m=25.1 mg/m^3, the deposition velocities are 1.06–1.94 times to those at C_m=11.3 mg/m^3, and for C_m=34.5 mg/m^3, they are 1.29–2.87 times. If current dimensionless deposition velocities in Table 2 are plotted against dimensionless relaxation time, the three lines show similar trend as straight lines. The slopes of the inclined lines are 0.496, 0.309 and 0.245 for C_m=11.3, 25.1 and 34.5 mg/m^3 respectively.

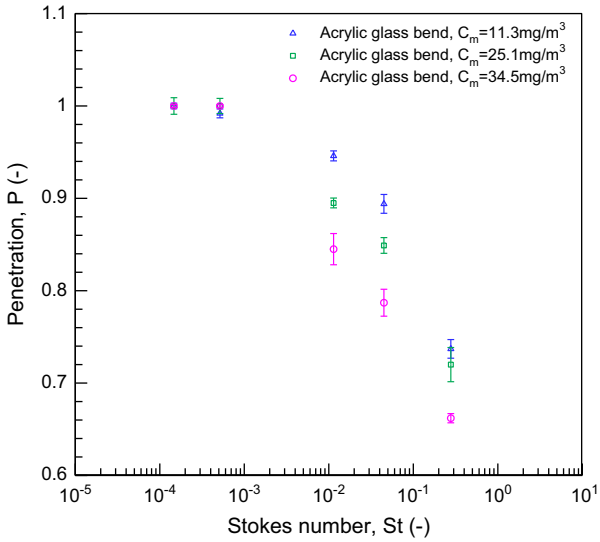

Fig. 2. Comparison of average particle penetration in a 90° acrylic glass bend under turbulent flow with different particle mass concentrations at bend inlet (De=9700).

Table 2
Measured average aerosol deposition velocities throughout 90° acrylic glass bends of rectangular cross section under turbulent flow under different particle mass concentrations at bend inlet (De=9700).

Inlet mass concentration (mg/m^3)	Particle size of APC channel (μm)	Relaxation time (dimensionless)	Measured deposition velocity (cm/s)	Deposition velocity (dimensionless)
11.3	5	0.337	1.34	9.05×10^{-2}
	10	1.33	2.64	0.178
	25	8.22	6.55	0.441
25.1	5	0.337	2.61	0.176
	10	1.33	3.76	0.253
	25	8.22	6.97	0.469
34.5	5	0.337	3.86	0.260
	10	1.33	5.30	0.357
	25	8.22	8.41	0.567

The moderate increasing portion of deposition velocity with the increase in inlet mass concentration is probably attributed to the increased particle accumulation on bend walls. Since the developing turbulence or disturbed flow can enhance the deposition even in straight ducts (Sippola & Nazaroff, 2005), the turbulences in bends and increased particle inlet concentration probably provide more opportunities towards enhanced deposition velocities when particles impact and deposit onto the bend wall (Tu et al., 2004). In other words, the developing and non-uniform distributed bend flow reinforces the concentration increase induced deposition in bends. The major mechanisms like centrifugal force and turbulent eddy in bends may have more chances to drive the particles onto bend walls when particle concentration increases (Breuer et al., 2006; Peters and Leith, 2004). Furthermore, an extra experiment was conducted with grease on bend walls under Case 4 condition for comparison. The measured results show a 10% increase of average deposition for particles of $St=1.14\times10^{-2}$. This result indicates that solid particles have bounced back into the flow without grease and influenced the bend outlet concentration. When there are more collisions with outer bend wall, rebounded particles will have less momentum and be easier to follow the air flow near outer wall since bend particle flow tends to assemble at this place (Jiang et al., 2011; Tian et al., 2008). As a result, concentration increase at inlet is observed to induce different concentration distribution at bend outlet and higher dimensionless concentration near outer bend wall as shown in Section 3.2.

As shown and analyzed above, the increasing concentrations provide more opportunities towards enhanced deposition velocities when particles impact and deposit onto bend walls. Although the rebounding particles may increase as well (Sun et al., 2011; Tu et al., 2004), the strengthened concentrations play the major role during the deposition and rebounding process with walls. Therefore, the deposition is enforced when particle inlet concentration increases as shown in Fig. 2 and Table 2. These statements can be more clearly explained from analytical analysis based on Eq. (3). The deposition velocity is defined in Eq. (3), where J_0 is the deposition flux of particles on a surface and average concentration C_{ave} is approximately the bend inlet concentration C_m. It is found in Fig. 2 that when average concentration C_{ave} or inlet concentration C_m increases ΔC_m, and thus particle deposition efficiency η or deposition flux J_0 onto bend wall also increases ΔJ_0. However, the result in Table 2 shows that deposition velocity V_d is definitely enhanced by ΔV_d due to inlet concentration C_m increases. Consequently, it can be inferred from Eq. (3) that the increase degree of total particle flux J_0 in the bend is much higher than the inlet concentration C_m increase. Based on these analyses, the following expression can be deducted from Eq. (3) as

$$J_0 = V_d C_m \tag{14}$$

$$\begin{aligned} J_0 + \Delta J_0 &= (V_d + \Delta V_d)(C_m + \Delta C_m) \\ &= V_d C_m + V_d \Delta C_m + C_m \Delta V_d + \Delta V_d \Delta C_m \end{aligned} \tag{15}$$

Eq. (15) minus Eq. (14) gives

$$\Delta J_0 = V_d \Delta C_m + C_m \Delta V_d + \Delta V_d \Delta C_m \tag{16}$$

From the above three equations, it is clear that flux increment ΔJ_0 is the integrated interaction of deposition velocity increment ΔV_d and inlet concentration increment ΔC_m, and therefore its increment degree is much larger than the other two increments.

Although current experiments are conducted with mass concentration from C_m=11.3 to 34.5 mg/m^3, it can be inferred that depositions under other unmeasured concentrations near current three ones can be calculated by interpolation accordingly. Current measurement results could help understand and evaluate the deposition change with inlet bulk particle concentration. This would also be a new reference to aerosol knowledge for users including engineers and designers.

3.2. Influence of inlet mass concentration on particle distribution

This subsection discusses the influence of inlet particle concentration on particle distribution at bend outlet because the particle deposition and rebounding within bends can affect the concentration distribution significantly. The effect of near wall particle concentration on particle deposition could be determined and analyzed through the concentration distributions. Dimensionless particle concentration distributions $\overline{C}_{r^*}$ against dimensionless wall distance r^* for a specific size are determined by Eqs. (8)–(10), and shown in Figs. 3–6 for particles of $St=5.15\times10^{-4}$–0.278. These experiments were conducted at the outlet symmetric line on the symmetric plane of a 90° acrylic glass bend with three different particle mass concentrations under Dean number $De=9700$. The corresponding experimental cases are no. 1–3 in Table 1.

As demonstrated in Fig. 3, particles of $d_{pn}=1$ μm or $St=5.15\times10^{-4}$ follow the mixing airflow extremely well to cross the bend at the bend outlet, and they are well-mixed. This statement is supported by the good agreement of larger than 97.2% with uniform dimensionless concentration $\overline{C}_u=1.00$ as shown in Table 3. This behavior is due to the extraordinarily low Stokes number $St=5.15\times10^{-4}$, which means that particles are diffusion dominated. This phenomenon provides a new angle of evidence on small particle flow mechanism which has been analyzed and proved in detail in previous bend deposition study (Sun et al., 2013). The uniform distributed concentration indicates that particles flowing throughout the

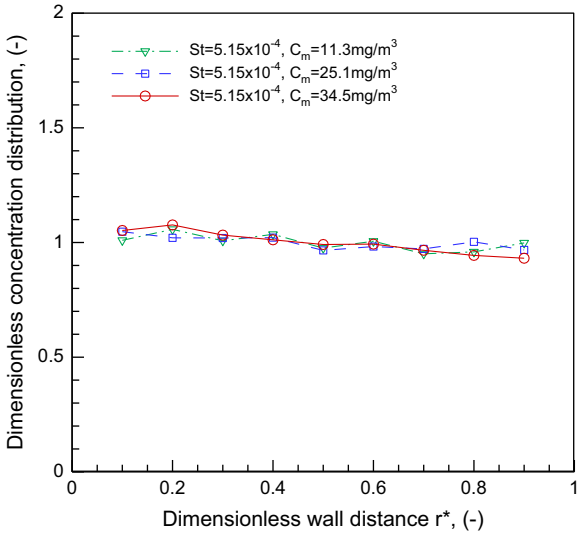

Fig. 3. Comparison of dimensionless particle concentration distribution $\overline{C}_{r*}$ at the outlet symmetric line of a 90° acrylic glass bend under turbulent flow with different particle mass concentrations C_m at bend inlet ($De=9700$, $St=5.15\times10^{-4}$).

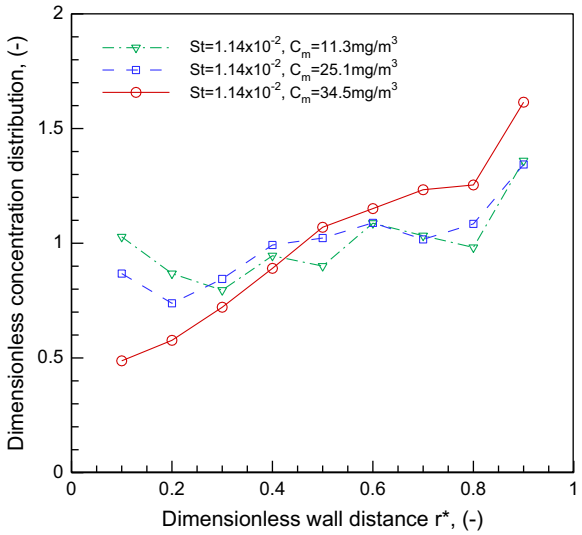

Fig. 4. Comparison of dimensionless particle concentration distribution $\overline{C}_{r*}$ at the outlet symmetric line of a 90° acrylic glass bend under turbulent flow with different particle mass concentrations C_m at bend inlet ($De=9700$, $St=1.14\times10^{-2}$).

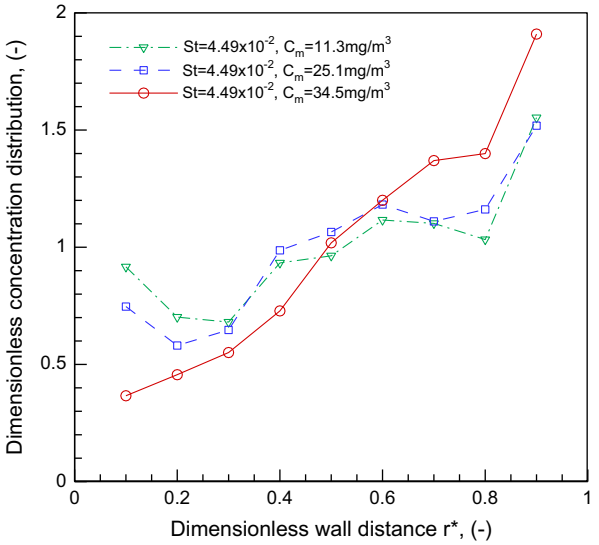

Fig. 5. Comparison of dimensionless particle concentration distribution $\overline{C}_{r*}$ at the outlet symmetric line of a 90° acrylic glass bend under turbulent flow with different particle mass concentrations C_m at bend inlet (De=9700, $St=4.49\times10^{-2}$).

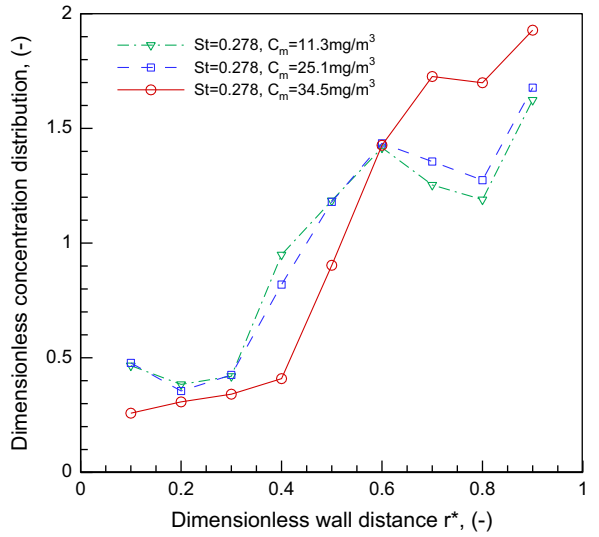

Fig. 6. Comparison of dimensionless particle concentration distribution $\overline{C}_{r*}$ at the outlet symmetric line of a 90° acrylic glass bend under turbulent flow with different particle mass concentrations C_m at bend inlet (De=9700, St=0.278).

Table 3
Average deviation of the dimensionless particle concentration distribution to the uniform distribution 1.00 at the bend outlet for different Stokes number (St) under different particle mass concentrations C_m and Reynolds numbers.

	Case 1 (%)	Case 2 (%)	Case 3 (%)	Case 4 (%)
$St=5.15\times10^{-4}$	2.6	2.5	3.8	13.7
$St=1.14\times10^{-2}$	11.3	12.4	29.5	35.0
$St=4.49\times10^{-2}$	17.9	23.1	42.2	47.5
St=0.278	38.4	42.8	61.8	69.2

bend are almost not influenced by bent wall surfaces. In other words, centrifugal force is marginal for particles of $St=5.15\times10^{-4}$. As regards to both the concentration distribution and particle penetration, inlet mass concentration differences have almost no contribution on this kind of small particles.

Starting from particles of d_{pn}=5 μm or $St=1.14\times10^{-2}$, dimensionless concentrations are not uniformly distributed at the bend outlet as shown in Figs. 4–6 and Table 3. Particles accumulate more near the outer bend wall and less near the inner

Table 4
Polarization factor of the dimensionless particle concentration distribution at the bend outlet for different Stokes number (St) under different particle mass concentrations C_m and Reynolds numbers.

	Case 1	Case 2	Case 3	Case 4
$St=5.15\times10^{-4}$	1.00	0.98	0.98	1.69
$St=1.14\times10^{-2}$	1.71	1.82	3.31	4.91
$St=4.49\times10^{-2}$	2.28	2.62	5.21	6.97
$St=0.278$	4.22	4.72	7.47	9.45

wall. Concentration distribution differences at the outlet are expanded with the increase of inlet mass concentration. In Fig. 4, dimensionless particle concentration $\overline{C}_{r^*}$ ranged from 0.796 to 1.36 for inlet mass concentration $C_m=11.3$ mg/m^3, while for $C_m=34.5$ mg/m^3, it was from 0.488 to 1.62. Compared to uniform distribution value 1.00, the average arithmetical deviations were estimated as 11.3%, 12.4% and 29.5% for $C_m=11.3$, 25.1 and 34.5 mg/m^3, respectively. This manner reveals that higher inlet mass concentration leads to higher concentration difference at bend outlet, and thus expedite the formation of concentration nonuniformity. The reason can be explained that when particles flow throughout the bend, centrifugal force and particle inertial drive more particles towards the outer bend wall under higher inlet concentration.

In Fig. 5, a broader range from 0.366 to 1.91 was observed for dimensionless particle concentration $\overline{C}_{r^*}$ under the highest inlet mass concentration $C_m=34.5$ mg/m^3. In Fig. 6, the largest range from 0.258 to 1.93 was found. These observations indicate that the nonuniform behavior is expanded when particle Stokes number increases. To discuss the large average deviation clearly, Table 3 was drawn to describe the nonuniformity comparisons in Figs. 3–6. It is easy to quantitatively examine the impelling effect of particle Stokes number St and inlet mass concentration C_m onto the concentration nonuniformity by the table. As stated above, for small particles of $St=5.15\times10^{-4}$, the nonuniformity due to St and C_m is neglectable, while for particles of $St=1.14\times10^{-2}$, only the influence of inlet mass concentration $C_m=34.5$ mg/m^3 is moderate. For even larger particles of $St=4.49\times10^{-2}$, the general effects of three inlet mass concentrations on concentration distribution nonuniformity are from moderate to significant. Finally, for the largest particles, all the inlet mass concentrations are significant to affect the concentration nonuniformity of polarization near inner and outer bend walls, as demonstrated in Table 3 and Figs. 4–6.

Furthermore, the increasing concentrations near the outer bend wall enhance the opportunities for particles to impact and deposit onto outer bend wall. The dimensionless concentration distributions in Figs. 4–6 show that particle concentration near the outer bend wall ($r^*=0.9$) is almost the highest and the one near inner wall ($r^*=0.1$) is nearly the lowest, especially for larger particles of $St\geq4.49\times10^{-2}$. Since current measurements were conducted at the symmetric centerline of the bend outlet, the deposition quantity rate $\int_{Ai}dJ$ near the inner wall and the one $\int_{Ao}dJ$ near the outer wall. n detail, the concentration C_{dAo} near the outer bend wall is higher than that C_{dAi} near the inner wall. According to the calculation in Table 2, the deposition velocity $V_{d,dAo}$ near the outer wall should be higher than that $V_{d,dAi}$ near the inner wall. As a result, the deposition quantity rate $\int_{Ao}V_{d,dAo}C_{dAo}\cdot dAo$ is larger than $\int_{Ai}V_{d,dAi}C_{dAi}\cdot dAi$. Based on experimental data analysis, this conclusion provides new evidence and a new angle of view to those phenomena predicted by Large Eddy Simulations (Berrouk & Laurence, 2008; Breuer et al., 2006).

As shown in Figs. 4–6, there are generally an apex and a concave point for $r^*=0.6$–0.8 for each curve. They are probably formed by the rebounding particles from the outer wall when particles impact onto it. Due to the rebounded particles, concentrations at $r^*=0.6$–0.7 usually form an apex, and those at $r^*=0.7$–0.8 exist a concave point. With the increase of inlet mass concentration, the values of the apex and concave increase as demonstrated in Fig. 4 to Fig. 6. However, for $C_m=34.5$ mg/m^3, the apex and concave points are not distinct compared to other two conditions. This phenomenon may be attributed to that the mainstream concentration C_m enhancement near the outer bend wall makes the apex and concave point be smoothed, which is caused by rebounding particles. Similarly, this explanation can also be applied to the apex, concave and smoothed concentration curve at the location $r^*=0.1$–0.3. In addition, the concentrations at $r^*=0.1$ for $C_m=11.3$ and 25.1 mg/m^3, are generally higher than that at $r^*=0.2$. Possible reasons for this observation could be the influence of secondary flow and streamwise eddies near the interior wall of bend outlet. Compared to circular bends, present ones with rectangular cross section are severely affected by secondary flow.

To further understanding the concentration nonuniformity in a new view angle, the concept of concentration polarization factor, PF, is proposed here as

$$PF=\frac{Max\left[\overline{C}_{r^*},r^*=\frac{m+1}{2(m+1)},\ldots,\frac{m}{m+1}\right]}{Min\left[\overline{C}_{r^*},r^*=\frac{1}{m+1},\ldots,\frac{m-1}{2(m+1)}\right]} \tag{17}$$

where the numerator is the maximum dimensionless concentration from bend central line to outer bend wall, the denominator is the minimum dimensionless concentration from bend central line to inner wall, and m is the measured point number. The concentration polarization factor, PF, is calculated out in Table 4 to compare the influence of Stokes number and inlet concentration. It shows that the PF ranges widely from 0.98 to 7.47. The table quantitatively demonstrates the fast increase of the polarization factor with particle Stokes number St and inlet concentration C_m, similarly as the trend of concentration average deviation in Table 3.

3.3. Influence of Reynolds number on concentration distribution

This section only presents the influence of Reynolds number on particle dimensionless concentration distribution at bend outlet since its influence on particle deposition and penetration has been investigated in the previous study (Sun et al., 2013). Although Reynolds number affects the average particle deposition trend marginally, it plays potentially significant role on the concentration distribution as described in detail below.

Figures 7 and 8 show the dimensionless concentration distribution more obviously for $St=5.15\times10^{-4}$–0.278 particles at the outlet of the bend under two Reynolds numbers, i.e. 17,900 and 35,600. Correspondingly, the Dean numbers are 9700 and 19,300 and the experimental cases are no. 1 and 4. The inlet mass concentrations are $C_m=11.3$ mg/m^3 for both cases. As shown in Fig. 7, fine particles of $St=5.15\times10^{-4}$ remains a uniform distribution as those in Fig. 3. However, larger particles of $St\geq4.49\times10^{-2}$ shifted from areas near inner wall to those near outer wall due to the bend effect and particle-bend impaction. Dimensionless particle concentration decreased to 0.384 approximately near the inner bend wall, and increased to 1.62 near the outer wall. With the existence of bend, particle concentration diverged in a significant degree for different particle diameters. This behavior is attributed to the influence of centrifugal force and inertia of the particle flow. These forces take significant effects for larger particles, yet have marginal influences on smaller ones. As the centrifugal force and

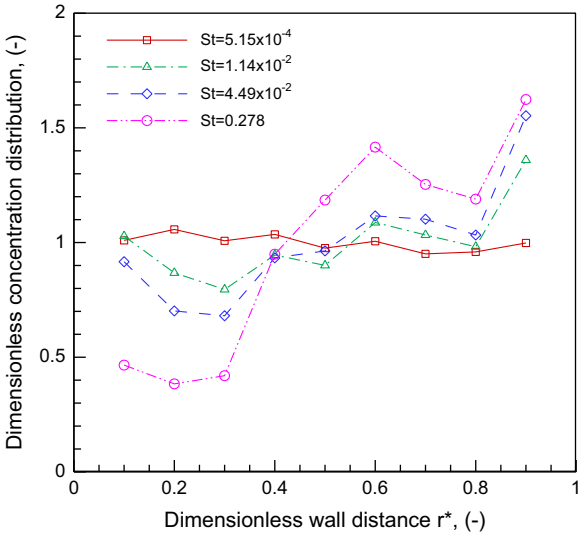

Fig. 7. Dimensionless concentration distribution $\overline{C}_{r*}$ against dimensionless wall distance r^* for the four particle Stokes numbers St at the outlet of bends under a lower Reynolds number $Re=17{,}900$ ($De=9700$, $C_m=11.3$ mg/m^3).

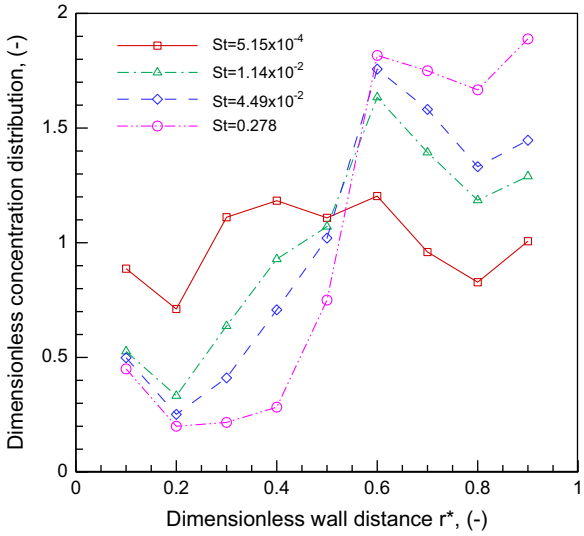

Fig. 8. Dimensionless concentration distribution $\overline{C}_{r*}$ against dimensionless wall distance r^* for the four particle Stokes numbers St at the outlet of bends under a higher Reynolds number $Re=35{,}600$ ($De=19{,}300$, $C_m=11.3$ mg/m^3).

inertia dominate large particle flow through the bend, they become two of the main factors to control the deposition process. The discussion can in return explain the reason of increasing large deposition portion for particles of large Stokes number in Fig. 2. Under relatively high Reynolds number $Re=35{,}600$, the behavior stated above is more distinct as shown in Fig. 8. Particle concentration of $St=5.15\times10^{-4}$ is not uniform along wall distances any more, but exhibit a certain fluctuations due to stronger turbulent eddies and/or secondary flows. Generally, the whole dimensionless concentrations for different particles increase near the outer bend wall and decrease near the inner wall. The dimensionless concentration ranged from 0.200 to 1.89 at the outlet. Most particles converged near the areas of outer bend wall, which partially support previous conclusion that deposited particles in bends accumulate mainly in the middle of bend outer wall (Breuer et al., 2006; Jiang et al., 2011), especially for larger Reynolds number. This behavior also shows a speeding-up formation of the so-called 'particle free zone' for larger Reynolds number near the bend interior wall as stated in previous numerical prediction (Sun et al., 2011; Tian et al., 2008). Besides the Reynolds number effect, both the increases of Stokes number and inlet concentration have accelerated the formation of the 'particle free zone' as demonstrated in Figs. 4–8.

Furthermore, it is interesting to find in Figs. 7 and 8 that an apex existed at $r^*=0.6$ and a concave point appeared at $r^*=0.8$ for all sizes of particles. This phenomenon is probably caused by the particle-wall collision effect at the outer bend wall. The rebounding particles form an apex at $r^*=0.6$ when the particle flow concentrates mostly on the outer bend wall due to the centrifugal effect. Particles of $St=0.278$ under $Re=35{,}600$ behave most obviously due to their largest inertia and centrifugal forces. From $r^*=0.4$ to 0.6, particle concentrations increase sharply for $St=1.14\times10^{-2}$–0.278 particles. The apex at $r^*=0.6$ was more obvious as rebounding particles increased with the increase of air velocity. Table 3 shows the average deviation of the concentration distribution from uniform distribution for experiment cases 1 and 4. Higher Reynolds number is found to have approximately 10–20% nonuniformity increase compared to the lower one. Table 4 presents the polarization for these two cases, and the factor *PF* under $Re=35{,}600$ is amplified to around 1.7–3.1 times compared to $Re=17{,}900$. With the increase of Reynolds number, the secondary flow in the bends will be much stronger. This strengthened secondary flow would probably lead to enhanced nonuniformity and *PF* factor. From the above two tables, the influence degree of Reynolds number is revealed to be severer than that of inlet concentration because average deviation and polarization factor enhancements under about two-time Reynolds number increase is larger than those under about three-time inlet concentration increase. In other words, Reynolds number is more important than inlet concentration for particle concentration distribution at bend outlet.

In this work, Reynolds number or corresponding Dean number influences the particle concentration distribution through the bend significantly, although it has marginal effect on averaged particle deposition trend. This behavior suggests that not only averaged deposition through the bends be considered an important factor for controlling particle pollutant, but also particle concentration distribution be another parameter for understanding the main accumulation location (Jiang et al., 2011), deposition distribution (Zhao & Wu, 2009) and even bend erosion place (Song et al., 1996) due to particle flow throughout the bends.

3.4. Influence of wall material on particle deposition

For precise comparison, only the bend was changed with different materials, and the other parts of the experiment setup were maintained the same. Typical acrylic clear glass and galvanized steel were chosen as the wall materials. The measurement cases 3 and 5 were conducted at a high inlet mass concentration of $C_m=34.5$ mg/m^3 under a low Dean number $De=9700$. Average particle penetrations for the two types of wall materials are shown in Table 5 under $De=9700$. For both materials, approximately, all the small particles penetrate the bends with Stokes number $St\leq5.15\times10^{-4}$. For other relatively larger particles with Stokes number from 0.0114 to 0.278, penetrations with steel bend are around 97.1% to 91.7% to those with glass steel bend. These penetration differences are not obvious between two material bends. For deposition velocity, however, these ratios are from 1.06 to 1.45 with the relaxation time $\tau_p^+=0.337$–8.22. This behavior means a larger difference of deposition velocity compared to penetrations, which reveals that deposition velocity is more sensitive to surface materials. The reason lies on that deposition velocity focuses on the near wall particle flux parameters, yet penetration concerns mainly on the mainstream flow properties. The exponential relationship between penetration and deposition velocity in bends (McFarland et al., 1997; Pui et al., 1987) weakens the material effect on penetration. In addition,

Table 5
Comparison of average particle penetration in 90° bends with two wall materials under turbulent flow ($C_m=34.5$ mg/m^3, $De=9700$).

Wall material	Particle Stokes number (St)	Measured average penetration (dimensionless)
Acrylic glass	1.14×10^{-2}	0.85
	4.49×10^{-2}	0.79
	0.278	0.66
Galvanized steel	1.14×10^{-2}	0.78
	4.49×10^{-2}	0.73
	0.278	0.64

differences between glass and steel materials depend primarily on the surface roughness, electrostatic, elastic and adhesive properties. Since the deposition velocity is sensitive to near wall flow and surface properties, surface material is an important factor to determine the accurate deposition velocity.

3.5. Influence of wall material on concentration distribution

Figures 9–14 show the concentration distribution comparison results at bend inlet and outlet with two kinds of bend wall materials, i.e. acrylic glass and galvanized steel. For inlet distribution, as presented in Figs. 9 and 10, these particles have very close distributions for glass and steel bends, with 95–98% consistency. The dimensionless concentrations near the inner bend wall are a little larger than those of other locations for particles of $St=4.49\times10^{-2}$ as shown in Fig. 10. This phenomenon has been found and partly supported by previous numerical modeling (Sun et al., 2011). Generally, the particle distributions of $St=5.15\times10^{-4}$ are the same for bend inlet and outlet except the point at $r^*=0.1$, as shown in Fig. 11. Similar distribution differences at this place of bend outlet can be found distinctly from the distributions of other diameter particles demonstrated in Figs. 12–14. The phenomenon could be seen as the shift of the particle concentration profile from inner wall and outer wall to the center mainstream, as demonstrated in the figures. The reason may be partly attributed to the low

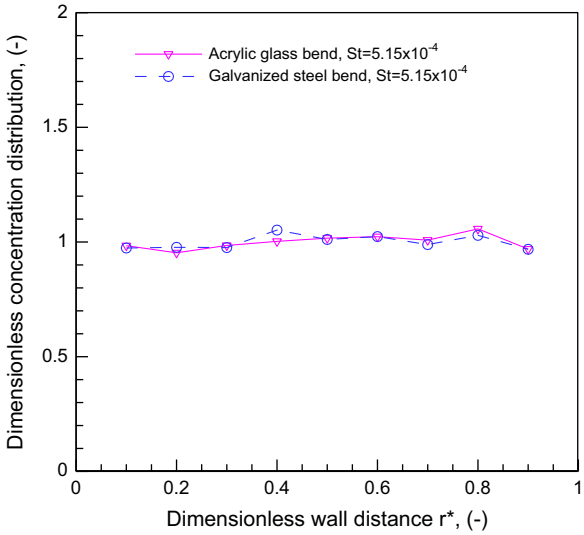

Fig. 9. Comparison of dimensionless particle concentration distribution at the inlet symmetric line of 90° bends with two wall materials under turbulent flow ($De=9700$, $C_m=34.5$ mg/m^3, $St=5.15\times10^{-4}$).

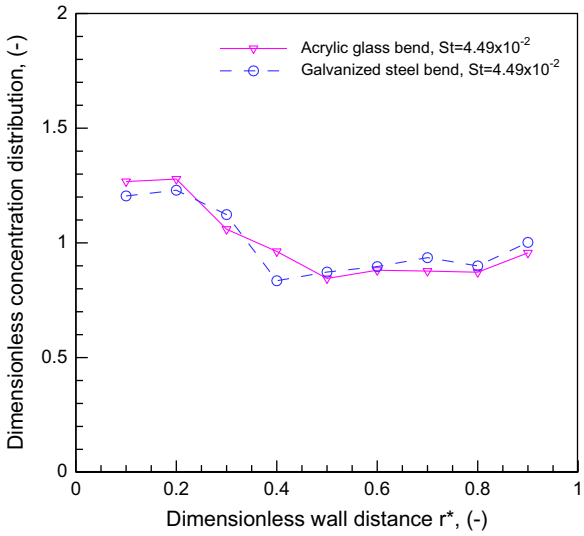

Fig. 10. Comparison of dimensionless particle concentration distribution at the inlet symmetric line of 90° bends with two wall materials under turbulent flow ($De=9700$, $C_m=34.5$ mg/m^3, $St=4.49\times10^{-2}$).

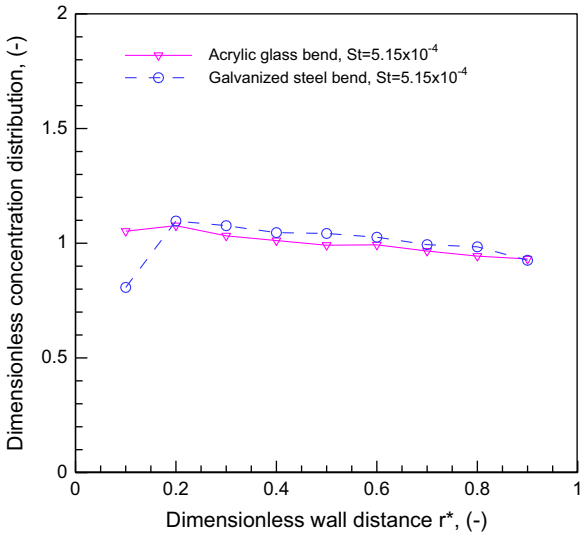

Fig. 11. Comparison of dimensionless particle concentration distribution at the outlet symmetric line of 90° bends with two wall materials under turbulent flow (De=9700, C_m=34.5 mg/m^3, St=5.15 × 10^{-4}).

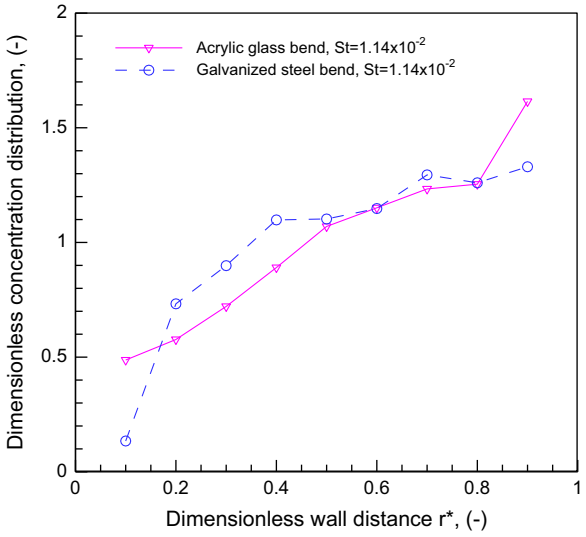

Fig. 12. Comparison of dimensionless particle concentration distribution at the outlet symmetric line of 90° bends with two wall materials under turbulent flow (De=9700, C_m=34.5 mg/m^3, St=1.14 × 10^{-2}).

rebounding and high adhering effect on the galvanized steel wall which retains more particles on its surface. Based on the particle-wall collision theory of Brach and Dunn (1998), Figs. 11–14 may also indicate that coefficients of restitution are different for particles bouncing from stainless steel and acrylic bend walls. As a result, particles with stainless steel concentrate more in the center areas of bend outlet section. In addition, material property differences on surface roughness and electrostatic property may provide another opportunity to influence the turbulent boundary layer flow or the particle-wall collision, and cause more depositions at the areas near the wall. Consequently, the particle concentrations with steel bend near the inner and outer wall are much lower than those with glass bend at a given inlet mass concentration. Furthermore, since the average depositions with steel bend are roughly higher than those with glass bend as shown in Table 5, the outlet concentrations with steel bend are inferred to be generally lower than those with glass bend at a same given inlet mass concentration according to Eq. (1). When the concentration distributions of a particle size are normalized by the average concentration of the size at bend outlet, the higher deposition near bend wall and lower average concentration at steel bend outlet contribute to generally higher dimensionless concentration near the bend center areas at r^*=0.3–0.6.

Figures 11–14 demonstrate markedly the deposition enhancement near the inner and outer bend wall with the increase of the particle diameter or particle Stokes number. The concentration ratios are listed in Table 6 to describe the concentrations with galvanized steel bend to those with acrylic glass bend at r^*=0.1 and 0.9. From the table and the

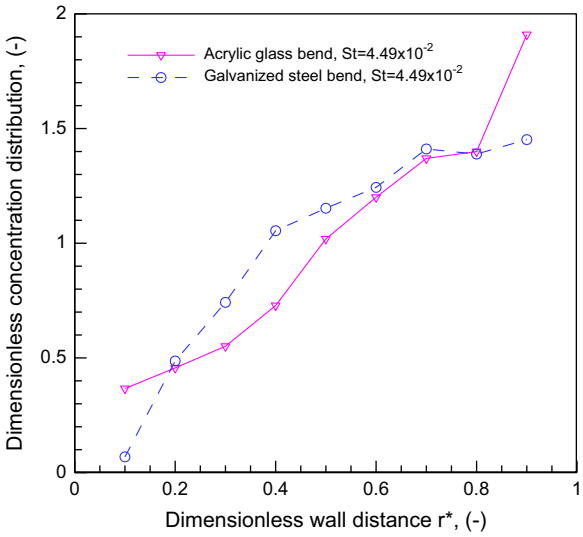

Fig. 13. Comparison of dimensionless particle concentration distribution at the outlet symmetric line of 90° bends with two wall materials under turbulent flow ($De=9700$, $C_m=34.5$ mg/m^3, $St=4.49\times10^{-2}$).

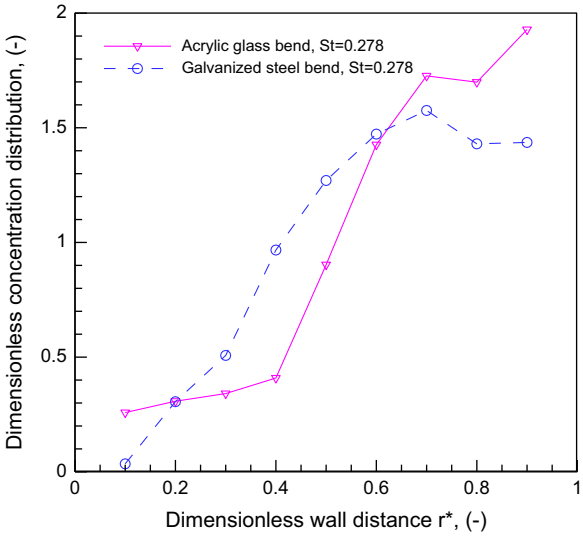

Fig. 14. Comparison of dimensionless particle concentration distribution at the outlet symmetric line of 90° bends with two wall materials under turbulent flow ($De=9700$, $C_m=34.5$ mg/m^3, $St=0.278$).

figures, it is easy to find that particle concentrations near the inner wall are decreasing rapidly to extremely small values. The dimensionless distribution values with galvanized steel bend at $r^*=0.1$ are 13.41%, 6.84% and 3.51% for Figs. 12–14 compared to the average concentration at bend outlet. These small portions of concentration can be considered as negligible distribution, especially the last two concentrations of $d_{pn}=10$ μm and 25 μm particles. The corresponding Stokes numbers for the two diameter particles are 0.0449 and 0.278. In consequence, there are areas without particles passing through near inner bend wall. These areas locate at least at $r^*\leq0.1$, which prove the existence of "particle free zone" (Breuer et al., 2006; Kliafas & Holt, 1987; Tian et al., 2008). For the measurements, the "particle free zone" exists between Stokes number 0.0449 and 0.278. Quantitatively, current experiments provide specific areas for particle of specific Stokes number range for "particle free zone" under the conducted measuring conditions. This finding is probably attributed to the consideration of particle-wall collision for solid particles (Tian et al., 2008).

Based on the experimental results, the "particle free zone" can be estimated as references for those predictions or models with similar conditions. For example, provided that the value 0.090 of dimensionless concentration is the threshold to define the "particle free zone", the location for a given diameter particle and the diameter for a given location could be calculated by interpolation. Based on the dimensionless concentrations at $r^*=0.1$ in Figs. 12–14, the following fitting equation can roughly express the relationship between dimensionless particle concentration $\overline{C}_{0.1}$ at $r^*=0.1$ and the

Table 6
Ratios of concentrations with galvanized steel bend to those with acrylic glass bend at near wall areas of $r^*=0.1$ and 0.9.

	$St=5.15\times10^{-4}$	$St=1.14\times10^{-2}$	$St=4.49\times10^{-2}$	$St=0.278$
$r^*=0.1$	0.767	0.276	0.187	0.135
$r^*=0.9$	0.994	0.824	0.760	0.745

corresponding particle Stokes number *St*.

$$\overline{C}_{0.1}=0.0159St^{-0.506} \tag{18}$$

The fitting r^2 value for this equation is 0.989, which is well-fitting between the equation and the experimental data. Given that the dimensionless concentration $\overline{C}_{0.1}=0.090$, Stokes number and particle diameter can be calculated as $St=0.0326$ and $d_{pn}=8.6$ μm, respectively. It means that particles larger than Stokes number $St=0.0326$ or particle diameter $d_{pn}=8.6$ μm will not flow through the locations smaller than $r^*=0.1$ under current conditions. These areas are so-called "particle free zone". For a given particle diameter, a simple interpolation method could estimate the range of "particle free zone". It is assumed that the threshold of the dimensionless concentration is $\overline{C}_{0.1}=0.090$. Using the values of dimensionless concentrations at $r^*=0.1$ and 0.2, the threshold locations are roughly computed to be $r^*=0.093$, 0.105 and 0.120 for $d_{pn}=5$, 10 and 25 μm particles, respectively. Particles of a specific diameter will form the "particle free zone" between the inner wall and the estimated location values. The findings and empirical equation above can benefit the understanding of the location of particle flow, guide the design of ventilation duct, help control the particle pollution through the ventilation system, and prevent the particle erosion on pneumatic flow ducts.

4. Conclusions

This article experimentally investigated particle concentration spatial distribution and deposition in 90° bends under five different conditions. Potential influencing factors are analyzed to reveal their impacts on particle distribution and deposition. The interaction between concentration distribution and deposition is discussed in detail. New phenomena, including particle nonuniformity, polarization factor, and 'particle free zone' in concentration, are observed and analyzed. In a summary, the following conclusions are obtained:

(1) Small particles with Stokes number $St\leq5.15\times10^{-4}$ had almost fully penetrations through the bend for all present experimental cases. The dimensionless deposition velocity ranged from 0.0905 to 0.567 against dimensionless relaxation time from $\tau_p^+=0.337$ to 8.22 for cases 1–3. Particle penetrations decreased moderately within 11% with the increase of inlet mass concentration. However, deposition velocity was enhanced from 1.29 to 2.87 times from $C_m=11.3$ to 34.5 mg/m^3. Increased particle inlet concentration provides an opportunity for more particles to impact and deposit onto the bend wall. It is concluded that the degree of average particle flux increase ΔJ_0 in the bend is much higher than the inlet concentration increase ΔC_m.

(2) On both the concentration distribution and particle penetration, inlet mass concentration differences have almost no influence for particles of $St=5.15\times10^{-4}$. These particles generally have uniform distribution at bend outlet under lower Dean number $De=9700$. Higher inlet mass concentration causes higher average concentration at bend outlet, higher concentrations near bend outer wall and lower ones near the inner wall. Higher inlet concentration and Stokes number expedites the developments of these kinds of concentration nonuniformity. Furthermore, apexes and concave points of the outlet distribution are formed by the rebounding particles from the outer wall. With the increase of inlet mass concentration, the values of the apex and concave point increase. To understand these large concentration differences between outer bend wall and inner one, polarization factor is defined to characterize the apex and concave degree.

(3) Reynolds number influences the aerosol concentration distribution significantly although it has been found to be minor factor to the average penetration and deposition. All Reynolds number, Stokes number and inlet concentration can accelerate the formation of 'particle free zone' near inner wall of bend outlet. However, Reynolds number has been proved to be a stronger parameter than inlet concentration shown from concentration nonuniformity and polarization factor.

(4) The penetration differences are not obvious between two material bends for at an inlet mass concentration of $C_m=34.5$ mg/m^3 under Dean number $De=9700$. However, deposition velocity is more sensitive to surface materials with an increase factor of 1.06–1.45 because of its sensitivity to surface structure and properties.

(5) For particle distribution, concentrations with galvanized steel bend near the inner and outer wall are considerably lower than those with acrylic glass one at a given inlet mass concentration, while the concentrations near the center mainstream areas are higher with steel bend. The dimensionless concentrations with steel bend at $r^*=0.1$ decrease fast against Stokes number, e.g. 0.0351, 0.0684 and 0.1341 to average concentration at bend outlet. These measured results provide direct concentration evidence of 'particle free zone'. Based on the experimental data, a rough estimation method and an empirical model are proposed to build the relationship among dimensionless outlet concentration, Stokes number and 'particle free zone' location.

Acknowledgment

This work was financially supported by The Hong Kong Polytechnic University through research grants A-PJ61 and A-PJ12. The authors would like to thank Professor S.C. Lee from the Department of Civil Engineering, Professor H.X. Yang from the Department of Building Services Engineering, The Hong Kong Polytechnic University and their group members for their kind help.

References

ASHRAE. (2009). ASHRAE handbook: fundamentals (SI ed.). American Society of Heating, Refrigerating and Air- Conditioning Engineers, Knovel, Atlanta, GA.

Berrouk, A.S., & Laurence, D. (2008). Stochastic modelling of aerosol deposition for LES of 90 degrees bend turbulent flow. *International Journal of Heat and fluid flow*, *29*, 1010–1028.

Brach, R.M., & Dunn, P.F. (1998). Models of rebound and capture for oblique microparticle impact. *Aerosol Science and Technology*, *29*, 379–388.

Breuer, M., Baytekin, H.T., & Matida, E.A. (2006). Prediction of aerosol deposition in 90 degrees bends using LES and an efficient Lagrangian tracking method. *Journal of Aerosol Science*, *37*, 1407–1428.

Chao, C.Y.H., & Tung, T.C. (2001). An empirical model for outdoor contaminant transmission into residential buildings and experimental verification. *Atmospheric Environment*, *35*, 1585–1596.

Jiang, H., Lu, L., & Sun, K. (2011). Experimental study and numerical investigation of particle penetration and deposition in 90 degrees bent ventilation ducts. *Building and Environment*, *46*, 2195–2202.

Jin, H.H., Fan, J.R., Zeng, M.J., & Cen, K.F. (2007). Large eddy simulation of inhaled particle deposition within the human upper respiratory tract. *Journal of Aerosol Science*, *38*, 257–268.

Kliafas, Y., & Holt, M. (1987). LDV measurements of a turbulent air-solid 2-phase flow in a 90-degree bend. *Experiments in Fluids*, *5*, 73–85.

Lai, A.C.K. (2002). Particle deposition indoors: a review. *Indoor Air*, *12*, 211–214.

Li, Y., Leung, G.M., Tang, J.W., Yang, X., Chao, C.Y.H., Lin, J.Z., Lu, J.W., Nielsen, P.V., Niu, J., Qian, H., Sleigh, A.C., Su, H.J.J., Sundell, J., Wong, T.W., & Yuen, P.L. (2007). Role of ventilation in airborne transmission of infectious agents in the built environment—a multidisciplinary systematic review. *Indoor Air*, *17*, 2–18.

Lin, J.Z., Lin, P.F., & Chen, H.J. (2009). Research on the transport and deposition of nanoparticles in a rotating curved pipe. *Physics of Fluids*, *21*, 122001-1–11.

Lin, J.Z., Zhang, W.F., & Yu, Z.S. (2004). Numerical research on the orientation distribution of fibers immersed in laminar and turbulent pipe flows. *Journal of Aerosol Science*, *35*, 63–82.

McFarland, A.R., Gong, H., Muyshondt, A., Wente, W.B., & Anand, N.K. (1997). Aerosol deposition in bends with turbulent flow. *Environmental Science & Technology*, *31*, 3371–3377.

Peters, T.A., & Leith, D. (2004). Measurement of particle deposition in industrial ducts. *Journal of Aerosol Science*, *35*, 529–540.

Pui, D.Y.H., Romaynovas, F., & Liu, B.Y.H. (1987). Experimental-study of particle deposition in bends of circular cross-section. *Aerosol Science and Technology*, *7*, 301–315.

Sippola, M.R. (2002). Particle Deposition in Ventilation Ducts. (Ph.D. dissertation). University of California, Berkeley, California.

Sippola, M.R., & Nazaroff, W.W. (2005). Particle deposition in ventilation ducts: connectors, bends and developing turbulent flow. *Aerosol Science and Technology*, *39*, 139–150.

Song, X.Q., Lin, J.Z., Zhao, J.F., & Shen, T.Y. (1996). Research on reducing erosion by adding ribs on the wall in particulate two-phase flows. *Wear*, *193*, 1–7.

Sun, K., Lu, L., & Jiang, H. (2011). A computational investigation of particle distribution and deposition in a 90° bend incorporating a particle-wall model. *Building and Environment*, *46*, 1251–1262.

Sun, K., Lu, L., Jiang, H., & Jin, H. (2013). Experimental study of solid particle deposition in 90° ventilated bends of rectangular cross section with turbulent flow. *Aerosol Science and Technology*, *47*, 115–124.

Tian, Z.F., Inthavong, K., Tu, J.Y., & Yeoh, G.H. (2008). Numerical investigation into the effects of wall roughness on a gas-particle flow in a 90 degrees bend. *International Journal of Heat and Mass Transfer*, *51*, 1238–1250.

Tu, J.Y., Yeoh, G.H., Morsi, Y.S., & Yang, W. (2004). A study of particle rebounding characteristics of a gas-particle flow over a curved wall surface. *Aerosol Science and Technology*, *38*, 739–755.

Wilson, S.R., Liu, Y.A., Matida, E.A., & Johnson, M.R. (2011). Aerosol deposition measurements as a function of Reynolds number for turbulent flow in a ninety-degree pipe bend. *Aerosol Science and Technology*, *45*, 364–375.

Yang, W., & Kuan, B. (2006). Experimental investigation of dilute turbulent particulate flow inside a curved 90 degrees bend. *Chemical Engineering Science*, *61*, 3593–3601.

Yang, Y., Sugimoto, J.D., Halloran, M.E., Basta, N.E., Chao, D.L., Matrajt, L., Potter, G., Kenah, E., & Longini, I.M. (2009). The transmissibility and control of pandemic Influenza A (H1N1) virus. *Science*, *326*, 729–733.

Yu, M.Z., Lin, J.Z., & Chan, T.L. (2008). Effect of precursor loading on non-spherical TiO_2 nanoparticle synthesis in a diffusion flame reactor. *Chemical Engineering Science*, *63*, 2317–2329.

Zaichik, L.I., Drobyshevsky, N.I., Filippov, A.S., Mukin, R.V., & Strizhov, V.F. (2010). A diffusion-inertia model for predicting dispersion and deposition of low-inertia particles in turbulent flows. *International Journal of Heat and Mass Transfer*, *53*, 154–162.

Zhang, H.F., & Ahmadi, G. (2000). Aerosol particle transport and deposition in vertical and horizontal turbulent duct flows. *Journal of Fluid Mechanics*, *406*, 55–80.

Zhang, K., Huang, L.Z., & Nie, D.M. (2010). Cylindrical microparticle transport and deposition from electrokinetic microflow in a 90 degree bend. *Mathematical and Computational Applications*, *15*, 822–827.

Zhang, Z., & Chen, Q. (2009). Prediction of particle deposition onto indoor surfaces by CFD with a modified Lagrangian method. *Atmospheric Environment*, *43*, 319–328.

Zhao, B., & Chen, J.J. (2006). Numerical analysis of particle deposition in ventilation duct. *Building and Environment*, *41*, 710–718.

Zhao, B., & Wu, J. (2007). Particle deposition in indoor environments: analysis of influencing factors. *Journal of Hazardous materials*, *147*, 439–448.

Zhao, B., & Wu, J. (2009). Effect of particle spatial distribution on particle deposition in ventilation rooms. *Journal of Hazardous materials*, *170*, 449–456.